CrystEngComm

RSC Publishing

PAPER

View Article Online
View Journal | View Issue

Orientation-dependent growth rate of crystalline plane study in electrodeposited Ni/Cu superlattice nanowires

Cite this: *CrystEngComm*, 2013, **15**, 4070

Shao Hui Xu, Guang Tao Fei,* Xiao Guang Zhu and Li De Zhang

A method of using the superlattice nanowire with epitaxial growth to study the relationship between the crystal orientation and corresponding growth rate for the electrodeposited nanowire is proposed. The relationship between growth rate and orientation of two metals Ni and Cu was studied through analysis of the epitaxial growth of Ni/Cu superlattice nanowires. Three samples with different periodic lengths were prepared by an electrodeposition method and analyzed to compare the segment lengths of nanowires with different crystalline orientations. The quantitative analysis result indicates that the growth rate of different planes exist $v_{(220)} : v_{(111)}$ = 1.25–1.31 for Ni, and $v_{(220)} : v_{(111)}$ = 1.32–1.41 for Cu, which qualitatively follow the Bravais rule. The quantitative analysis for the relationship between growth rate and orientation is important for the effective control of the uniform growth of the electrodeposited nanowires.

Received 3rd February 2013,
Accepted 18th March 2013

DOI: 10.1039/c3ce40231b

www.rsc.org/crystengcomm

Introduction

Nanowires as the main structure of a one-dimensional nanostructure have been prepared and studied intensively owing to their novel physical properties and fascinating potential applications in future nanodevices.[1–5] At present, template-assisted electrodeposition is regarded as a simple and flexible method for the preparation of nanowires. Many kinds of nanowires, including metals,[6–10] semiconductors,[11–15] and conductive polymers[16] have been successfully fabricated in the hole of an anodic aluminum oxide (AAO) template by the electrodeposition method. However, during the growth process of the nanowires in the AAO, it was found that the nanowires lengths in different holes were different.[17–20] Trahey deposited Bi_2Te_3 nanowires in the AAO template, and observed that the nanowire lengths in the pores were inconsistent, he thought that the inhomogenous nucleation and growth of nanowires in different holes were the main factors causing the above phenomenon.[17] In addition, Dou prepared a Bi/BiSb superlattice nanowire with the electrodeposition method and found that the nanowires in the same sample had different segment lengths.[21] He thought this was because nanowires with different growth orientations had different growth rates.

Whether or not the growth rate of deposited nanowires depends on their growth orientation, and how the quantitative relationship between growth rates of crystalline planes with different orientations in nanowires works are questions worth exploring, which are important for an in-depth understanding of the growth of the electrodeposited nanowire and finally for achieving controllable preparation. Unfortunately, up to now, there have been almost no experimental studies on the relationship between the crystal orientation and the corresponding growth rate for nanowires prepared by electrodeposition because there is no good method. For ordinary electrodeposited nanowires, the nanowire length is related to both rates of nucleation and growth under uniform pore size.[22,23] Therefore, it is hard to study the exact relationship between crystal orientation and corresponding growth rate by comparing the lengths of the nanowires with different growth orientations because the rate of nucleation also needs to be taken into consideration. Here, a new method of using the structure of superlattice nanowire with epitaxial growth to study the relationship between the crystal orientation and corresponding growth rate for the electrodeposited nanowire was proposed. In the superlattice nanowire with epitaxial growth, each segment grows directly on a similar crystal surface and does not undergo the nucleation process. Therefore, each segment length is just related to the growth rate. In addition, we prepared many periods of segments in each nanowire and used the statistical average value of several segment lengths as the value of the segment length. By comparing the periodic length of each segment in the nanowires with different orientations, we can derive the relationship between orientation and growth rate easily.

Both Ni and Cu are of face-centered cubic crystal structure, and the cell parameters (a = 0.3523 nm for Ni, a = 0.3615 nm for Cu, a is the cell parameters) are quite close, when these two metals deposited alternately, which is beneficial for epitaxial growth, thus satisfying the requirements of research and

Key Laboratory of Materials Physics and Anhui Key Laboratory of Nanomaterials and Nanotechnology, Institute of Solid State Physics, Hefei Institutes of Physical Science, Chinese Academy of Sciences, P. O. Box 1129, HeFei 230031, P. R. China. E-mail: gtfei@issp.ac.cn; Fax: +86-551-5591434; Tel: +86-551-5591453

becoming our study aim. In this paper, we prepared three kinds of Ni/Cu superlattice samples with different segment lengths and carried out a study on the orientation-dependent growth rate of the crystal plane. Moreover, a quantitative relationship between growth rates of two different crystal planes is given.

Experimental

The AAO templates were prepared *via* a two-step anodization process as the reported previously.[24] After anodization, the back aluminum was removed in a saturated $CuCl_2$ solution, and then the barrier was dissolved in 5 wt% phosphoric acid solution at 40 °C for 25 min. The obtained AAO templates had a pore size of about 50 nm. An Au layer about 200 nm thickness was sputtered onto the bottom of the double-opened AAO as the working electrode.

Two elements of Ni and Cu were electrodeposited alternately in different electrolytic cells respectively, thus the deposition condition for each segment can be controlled independently. After each segment deposition, there was a cleaning process, of which the AAO was rinsed in deionized water to remove residual electrolyte from the pores. All the processes, including electrodeposition and cleaning, were carried out by a programmed device.[25] The electrolyte used for deposition of Ni consisted of 0.38 M $NiSO_4{\cdot}6H_2O$, 0.12 M $NiCl_2{\cdot}6H_2O$, and 0.5 M H_3BO_3, and the pH value was adjusted to about 2.5 with 1 M H_2SO_4; the electrolyte used for Cu deposition contains 0.2 M $CuSO_4{\cdot}5H_2O$ and 0.5 M H_3BO_3 with a pH value also about 2.5 adjusted by 1 M H_2SO_4. The deposition voltages for Ni and Cu are about 1.9 V and 0.8 V, respectively. Three Ni/Cu samples with different segment lengths were prepared. The deposition time for Ni and Cu in the three samples, named sample 1, sample 2 and sample 3, were 15 s/60 s, 45 s/45 s, and 75 s/30 s, respectively.

The morphology of the nanowires was characterized by a field emission scanning electroscope microscope (FE-SEM). The crystalline structure of the nanowires was studied by an X-ray diffractometer (Philips X'Pert) with a Cu $K\alpha_1$ radiation (λ = 1.54056 Å), transmission electron microscope (TEM, JEOL-2010) and selected area electron diffraction (SAED). The composition dispersion was investigated by energy dispersive X-ray spectroscopy (EDS) element mapping analysis. For the TEM observation, the AAO was dissolved with 5 wt% NaOH solution for about 25 min to make sure all the nanowires were completely released from the template, and then the specimens were cleaned thoroughly by deionized water and absolute ethanol, respectively, several times, and at last ultrasonically dispersed in ethanol.

Results and discussion

Fig. 1 shows the FE-SEM image of Ni/Cu superlattice nanowire arrays released from AAO template, in which we can see clearly these nanowires displaying the periodic contrast changes and uniform morphology. Fig. 2 is the scheme of the XRD measurement setup. The XRD we measured here corresponds to the collective result of the nanowires in the sample. These nanowires filled in the pores of AAO are parallel and independent of each other. In the process of the measurement, the sample is kept horizontal and remained immobile in the same place, while the incident X-ray and diffracted X-ray move toward each other synchronously. In this case, only diffraction peaks of the crystal planes parallel to the sample surface can be detected and the diffraction peaks in the XRD pattern correspond to the growth plane which is perpendicular to the axial direction of the nanowire. Fig. 3 shows the typical XRD patterns of Ni/Cu superlattice nanowire arrays of the three samples, in which we may find that three growth planes appear and can be indexed to (111), (200) and (220) for both elements Cu and Ni, this means that in each sample there are three different growth orientations of nanowires, and their growth orientation can be indexed as [111], [200] and [220], which is further proved in the following TEM analysis. Besides, it can be seen with each Cu diffraction peak, there exists an accompanying Ni diffraction peak with the same orientation, showing Ni segments and Cu segments tend to grow with the same crystalline orientation in the Ni/Cu superlattice nano-

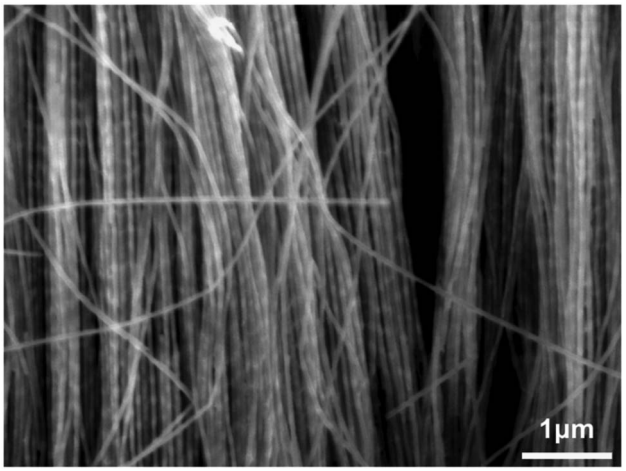

Fig. 1 The FE-SEM images of nanowire released from the AAO template.

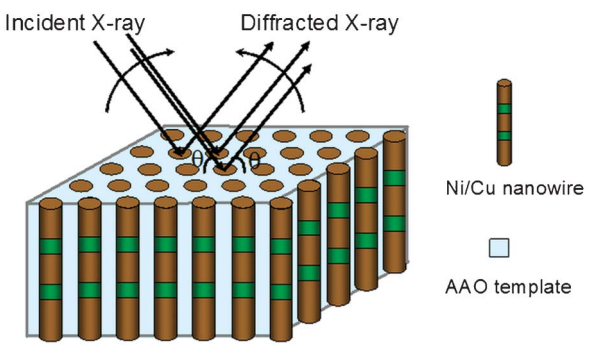

Fig. 2 Scheme of the XRD measurement set-up.

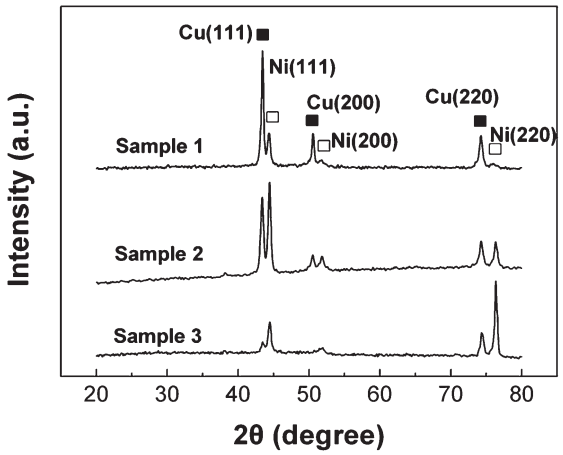

Fig. 3 The XRD patterns of Ni/Cu superlattice nanowire arrays in the three samples with different segment lengths.

wires, which has also been proved in the following context. This growth pattern is close to epitaxial growth. The fact that different growth orientations of nanowires appear in each sample is beneficial to comparing the segment length of nanowires with different orientations in the same sample and thus studying the relationship between orientation and growth rate.

The electrodeposition of each nanowire experiences a process from nucleation to growth. During the nucleation stage, different orientations of grains stacked to form the polycrystalline segment. With growth of the grains, the crystal grain of a certain orientation dominates the growth and forms a single crystal. In our experiment, the deposition parameters for each element can be controlled independently, allowing us to deposit each segment much closer to the thermodynamic equilibrium condition. Therefore, after the monocrystalline fill the radial direction of the hole, the Ni and Cu subsequently deposited would grow along the orientation of the monocrystalline and no longer change under the thermodynamic equilibrium conditions. At the initial stage of deposition, the deposition condition is not completely stable, therefore the initial deposition environment is not completely the same for each pore, which leads to the crystalline orientations of the initial monocrystalline segment in different pores being different, so the growth orientations of the Ni/Cu nanowires in the pores are not completely the same. In the following study, we used the TEM method to select two nanowires with [111] and [220] orientations respectively in each sample for analysis.

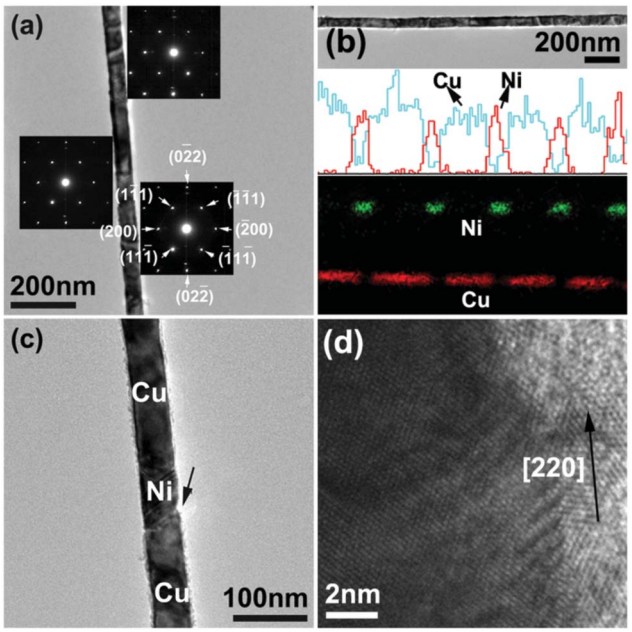

Fig. 4 (a) The TEM image of a single Ni(96 nm)/Cu(246 nm) nanowire in sample 1, the inset is the corresponding SAED of three areas on the nanowire. (b) The corresponding EDS line profile and element mapping image for the same nanowire. (c) The TEM image of the magnified interfaces of the nanowire. (d) The HR-TEM image of the interface marked by an arrow in (c).

Fig. 4(a) shows the TEM image of a single nanowire in sample 1, the inset corresponds to the SAED of three different positions of the nanowire containing Ni segment, Cu segment and the interface between segments. From the SAED patterns we can judge that the growth orientation of this nanowire is [220]. The crystalline structure of Ni and Cu both are FCC, and the lattice fringes are similar for the same crystal face, therefore diffraction patterns at the interface coming from Cu and Ni almost overlap, displaying almost one set of diffraction points. Fig. 4(b) shows the TEM image of the single nanowire, the corresponding EDS line profile and element mapping images. It can be seen that the nanowire grows with two elements Ni and Cu in periodic alternation. In addition, based on the TEM image, the EDS line profile and element mapping, we can obtain the segment lengths of Ni and Cu as about 96 nm and 246 nm, respectively. All the values of the segment length in this text are the mean values of the single measurement of several segment lengths measured as mentioned previously.[25] Fig. 4(c) displays the magnified TEM image of the interfaces on the nanowire, and the HR-TEM image of the interface marked by the arrow is given in Fig. 4(d). The arrow in Fig. 4(d) marks the axial orientation of nanowire, the lattice fringe image indicates the growth orientation of the nanowire is [220], which is consistent with the SAED results.

Fig. 5(a) gives the TEM image of another nanowire from sample 1 and the insets show the corresponding SAED patterns of three different positions on the nanowire. The diffraction patterns indicate that the growth orientation of nanowire is [111]. Fig. 5(b) shows the corresponding EDS line profile and elemental mapping image, from which we can judge the segment lengths of Ni and Cu are about 74 nm and 186 nm, respectively. Fig. 5(c) displays the magnified TEM image of the interfaces, and Fig. 5(d) gives the corresponding HR-TEM image of the interface marked by an arrow. The arrow in Fig. 5(d) marks the axial orientation of the nanowire, the crystalline plane perpendicular to the growth orientation of

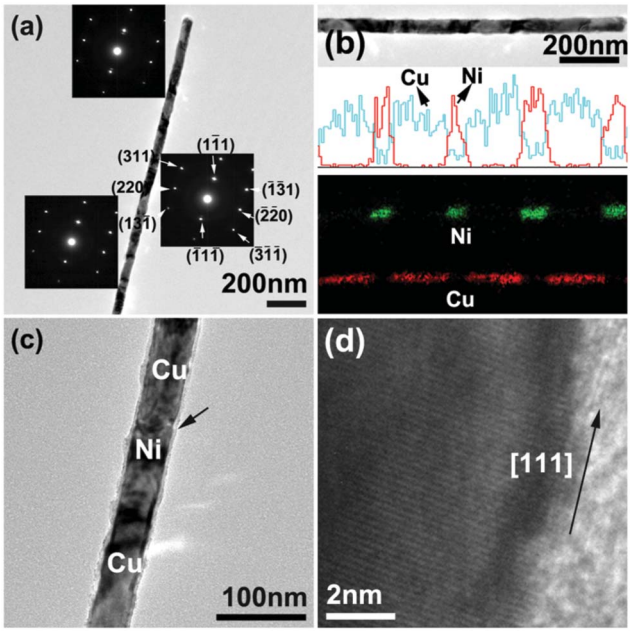

Fig. 5 (a) The TEM image of a single Ni(74 nm)/Cu(186 nm) nanowire in sample 1, the inset is the corresponding SAED of three areas on the nanowire. (b) The corresponding EDS line profile and element mapping image for the same nanowire. (c) The TEM image of the magnified interfaces of the nanowire. (d) The HR-TEM image of the interface marked by an arrow in (c).

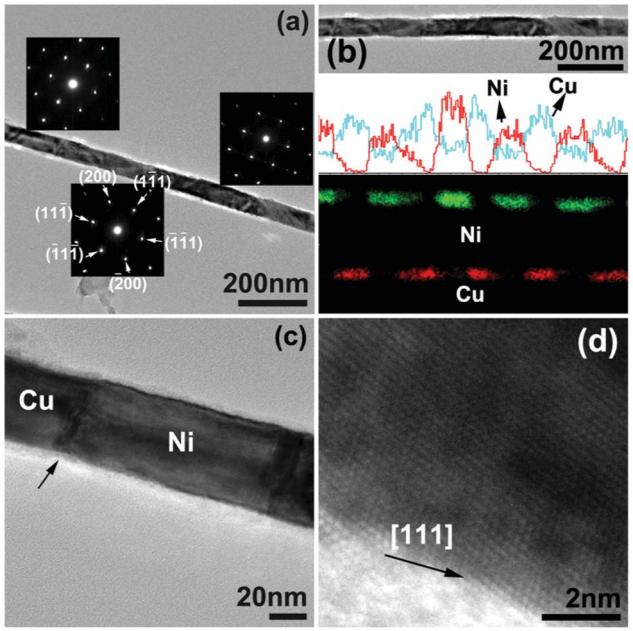

Fig. 7 (a) TEM image of a single nanowire Ni(119 nm)/Cu(85 nm) in sample 2, the inset is the corresponding SAED of three areas on the nanowire. (b) The corresponding EDS line profile and elemental mapping image for the same nanowire. (c) The TEM image of the magnified interfaces of the nanowire. (d) The HR-TEM image of the interface marked by an arrow in (c).

this nanowire is (111), consistent with the result of SAED. Comparing the two nanowires in sample 1, we may note that the segment lengths are different for the two nanowires with different growth orientations, which indicates the growth rates are different for the nanowires with different orientations in the same sample.

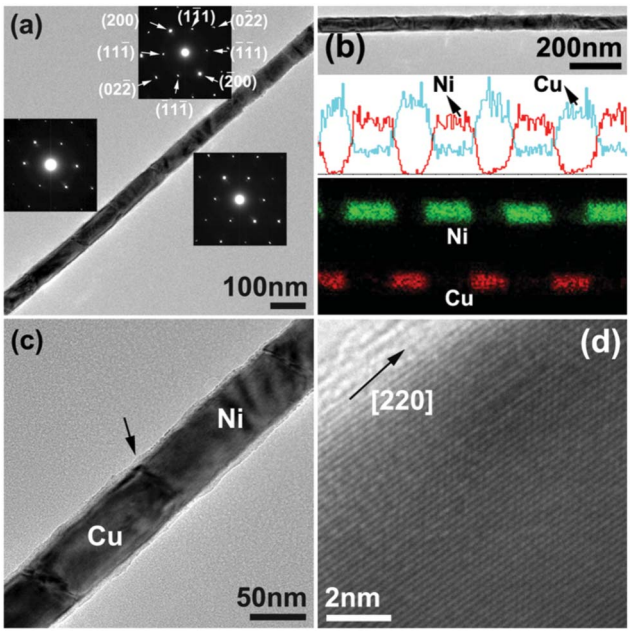

Fig. 6 (a) TEM image of single nanowire Ni(157 nm)/Cu(120 nm) in sample 2, the inset is the corresponding SAED of three areas on the nanowire. (b) The corresponding line profile and EDS elemental mapping image. (c) The TEM image of the magnified interfaces. (d) The HR-TEM image of the interface marked by an arrow in (c).

Similarly, we chose two Ni/Cu superlattice nanowires with growth orientations [220] and [111], respectively, in sample 2 for analysis. Fig. 6(a) shows the TEM image of one nanowire, and the insets are the corresponding SAED patterns of three different positions of the nanowire, from which it can be judged that the growth orientation of this nanowire is [220]. Fig. 6(b) displays the corresponding EDS line profile and elemental mapping image, from which we can derive the segment lengths of Ni and Cu are about 157 nm and 120 nm, respectively. Fig. 6(c) and (d) show the magnified TEM image of the interfaces and the corresponding HR-TEM image of the interface labeled by an arrow, respectively. The arrow in Fig. 6(d) marks the axial orientation of the nanowire, the lattice fringe in HR-TEM image is consistent with the SAED result, showing the growth orientation of this nanowire is [220]. Fig. 7 gives the characterization result of another nanowire in sample 2 containing the TEM image, SAED patterns, the corresponding EDS line profile and elemental mapping image, and the HR-TEM image of the interface. By analysis of the TEM image and the EDS elemental mapping image, the segment lengths of Ni and Cu which are about 119 nm and 85 nm respectively can be obtained. The SAED patterns and the HR-TEM images both show the growth orientation of the nanowire is [111].

Moreover, similar analysis for nanowires in sample 3 was carried out. Fig. 8(a)–(d) show the SAED patterns of a single

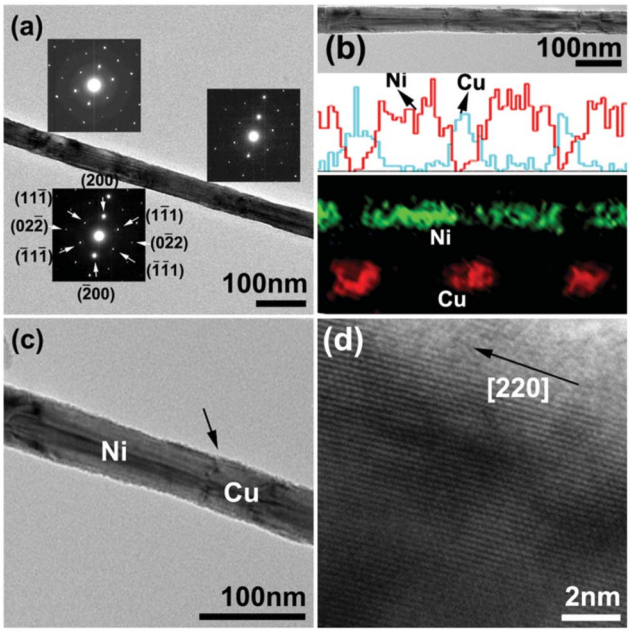

Fig. 8 (a) TEM image of a single nanowire Ni(176 nm)/Cu(68 nm) in sample 3, the inset is the corresponding SAED of three areas on the nanowire. (b) The corresponding EDS line profile and elemental mapping image for the same nanowire. (c) The TEM image of the magnified interfaces of the nanowire. (d) The HR-TEM image of the interface marked by an arrow in (c).

nanowire in sample 3, the corresponding EDS line profile and elemental mapping image, the magnified TEM image of a typical junction and the HR-TEM image of the interface,

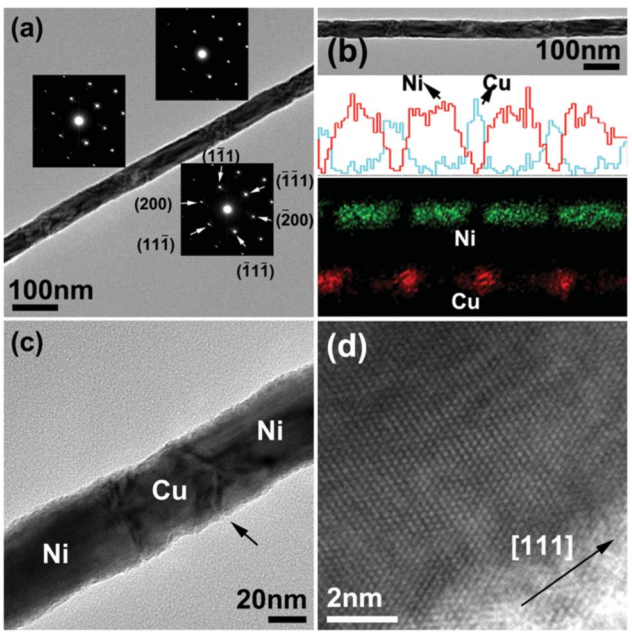

Fig. 9 (a) TEM image of a single nanowire Ni(141 nm)/Cu(50 nm) in sample 3, the inset is the corresponding SAED of three areas on the nanowire. (b) The corresponding EDS line profile and element mapping image for the same nanowire. (c) The TEM image of the magnified interfaces of the nanowire. (d) The HR-TEM image of the interface marked by an arrow in (c).

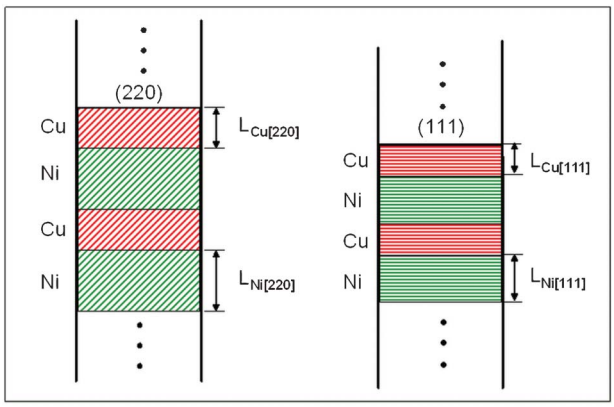

Fig. 10 The growth process diagram of Ni/Cu superlattice nanowires with growth planes (220) and (111), respectively.

respectively. The above characterizations indicate the nanowire grows along orientation [220], and the segments lengths are about 176 nm for Ni and 68 nm for Cu. In the same way, another nanowire in sample 3 was analyzed as shown in Fig. 9, in which the SAED patterns, EDS line profile and elemental mapping image, magnified TEM image of the interface and the corresponding HR-TEM are given. From the characterization results of Fig. 9 we can conclude that this nanowire grows along [111] and the segment lengths of the nanowire are about 141 nm for the Ni segment and 50 nm for the Cu segment respectively, different from the element segment lengths of the nanowire with [220] orientation in sample 3.

The detailed characterization results of the three samples are described above. The SAED patterns from the middle position of the Ni segment and the Cu segment as well as their interface are quite similar, and the HR-TEM image of the interface implies the lattice fringe image is almost constant from one metal to the other. All of these experimental results indicate the superlattice nanowires comply with epitaxial growth. The growth process can be described by the schematic diagram in Fig. 10. Since the crystalline lattice of two metals containing Ni and Cu are quite close, when these two metals grow alternately, the metal below can act as the substrate to induce the other metal to grow with the same crystalline direction, and finally form the epitaxial growth.

It can be seen from Fig. 4–9 that the segment lengths of the Ni/Cu superlattice with [220] orientation are different to that of the Ni/Cu superlattice with [111] orientation. Here, we define the segment lengths of Cu and Ni as $L_{Cu[220]}$ and $L_{Ni[220]}$ in [220] orientation of Ni/Cu nanowire, and $L_{Cu[111]}$ and $L_{Ni[111]}$ in [111] orientation of Ni/Cu nanowire, respectively, as shown in Fig. 10. Because the superlattice nanowires follow epitaxial growth, the segment length is only related to the growth rate. Therefore, we can obtain the relationship of the growth rate between planes (220) and (111) for Cu by comparing $L_{Cu[220]}$ and $L_{Cu[111]}$, and obtain the relationship of growth rates between planes (220) and (111) for Ni by comparing $L_{Ni[220]}$ and $L_{Ni[111]}$, respectively.

Table 1 The segment lengths of Ni and Cu in three samples and the ratio of growth rates of different crystal planes

Sample		[220]	[111]	Ratio
1	Ni	96 nm	74 nm	$v_{(220)} : v_{(111)} = 1.29$
	Cu	246 nm	186 nm	$v_{(220)} : v_{(111)} = 1.32$
2	Ni	157 nm	119 nm	$v_{(220)} : v_{(111)} = 1.31$
	Cu	120 nm	85 nm	$v_{(220)} : v_{(111)} = 1.41$
3	Ni	176 nm	141 nm	$v_{(220)} : v_{(111)} = 1.25$
	Cu	68 nm	50 nm	$v_{(220)} : v_{(111)} = 1.36$

Table 1 lists the segment lengths of the Ni and Cu with different growth orientations in the three samples, based on which we calculated the ratio between growth rates of different crystalline planes. In sample 1, the segment lengths of Ni are 96 nm for [220] orientation and 74 nm for [111] orientation, respectively. Therefore, the growth rates of the two crystalline planes (220) and (111) of Ni nanowire exist in such a relationship as: $v_{(220)} : v_{(111)} = 1.29$. For metallic Cu, the segment lengths are 246 nm for [220] orientation and 186 nm for [111] orientation, respectively. Therefore, the growth rates for the two different crystalline planes of Cu nanowire exist in such a relationship as: $v_{(220)} : v_{(111)} = 1.32$. In sample 2, the segment lengths of metallic Ni are respectively 157 nm for [220] orientation and 119 nm for [111] orientation, so the growth rates of the two different crystalline planes (220) and (111) exist in such relationship as: $v_{(220)} : v_{(111)} = 1.31$. For metallic Cu, the segment lengths are 120 nm for [220] orientation and 85 nm for [111] orientation, respectively, so the relationship $v_{(220)} : v_{(111)} = 1.41$ was obtained. In the same way, comparing the segment lengths of the two metals with different orientations of [220] and [111] in sample 3, we get $v_{(220)} : v_{(111)} = 1.25$ for Ni and $v_{(220)} : v_{(111)} = 1.36$ for Cu.

The above calculated results demonstrate that the growth rate of the crystalline plane (220) is larger than that of the crystalline plane (111) for both Ni and Cu nanowires prepared by electrodeposition, which is consistent with the Bravais rule.[26] The Bravais rule shows that during the growth process of the crystal, the growth rate of the crystalline plane is inversely proportional to the lattice density in the plane, which can be described using the schematic diagram in Fig. 11. AB, BC and CD are three net planes perpendicular to the paper plane. Among these three net planes, the AB plane has the largest density of node, and the largest plane separation; its surface energy is the lowest. Therefore, the attraction ability of this net plane to the outside atom is small which leads to a low growth rate. Compared with the AB plane, the CD plane has a lower density of node, a lower plane separation and a higher surface energy, and the growth rate is higher. The BC plane has the smallest density of node, the smallest plane separation, and the surface energy is the highest. When the new atom outside falls on the crystal, it will most likely adhere to position 1 in order to decrease the surface energy, so the BC crystalline plane will grow the fastest. In our study, the two nanowires analyzed in each sample grow along the crystal orientation [220] and [111], respectively. Due to the lattice

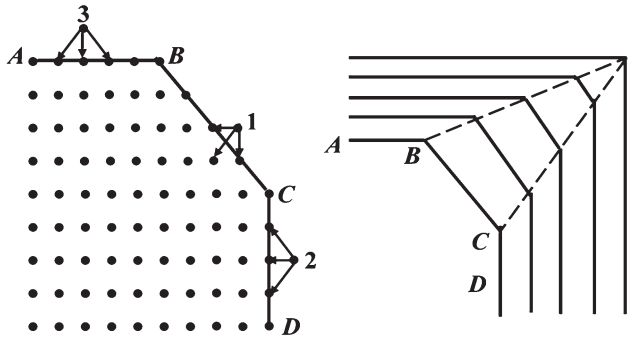

Fig. 11 The lattice density and growth rate of the crystalline plane.

density ρ of plane (220) is smaller than that of plane (111), that is $\rho_{(220)} < \rho_{(111)}$, and the surface energy of (220) plane is higher than that of (111) plane, therefore, the growth rates v of this two planes should follow $v_{(220)} > v_{(111)}$ according to the Bravais rule. Our calculated result from the experiment value is consistent with the Bravais rule, indicating the growth process of the nanowire electrodeposited in the AAO template complies with the Bravais rule. Besides, comparing the analysis result of the growth rate of the two metal nanowires, we may find that the ratios of growth rates of the two planes (220) and (111) are almost equal for both Ni and Cu, the quantitative analysis results indicate that the growth rate of two planes exist $v_{(220)} : v_{(111)} = 1.25$–$1.31$ for Ni, and $v_{(220)} : v_{(111)} = 1.32$–$1.41$ for Cu.

This study provides experimental data for the quantitative analysis of the relationship between growth rates of different crystalline planes in electrodeposited Ni and Cu nanowires in the AAO template, which is important for understanding the growth of nanowires and thus of benefit for controlling the nanowire length with uniformity. Moreover, the method provided here is not restricted by the crystal structure of the nanowires. As long as the epitaxial growth of superlattice nanowires with different growth orientations in one sample for other crystal planes are obtained, the quantitative relationship between growth rates of the different crystal planes can then be studied.

Conclusions

By means of superlattice nanowires, we analyzed the growth rates of Ni and Cu nanowires electrodeposited with different orientations. It is found that the relationship between growth orientation and growth rate of crystalline planes follow the Bravais rule. Quantitative analysis results indicate that the growth rate of different planes exist $v_{(220)} : v_{(111)} = 1.25$–$1.31$ for Ni, and $v_{(220)} : v_{(111)} = 1.32$–$1.41$ for Cu. This work is important for understanding the growth of the nanowire deposited in the pore of the template and thus the control of the nanowire length with uniformity.

Acknowledgements

This work was supported by National Basic Research Program of China (973 Program) (No. 2012CB932303), the National Natural Science Foundation of China (Nos. 51171176, 11204307), and China Postdoctoral Science Foundation (No. 2012M511948).

Notes and references

1 X. Wang, J. Song, J. Liu and Z. L. Wang, *Science*, 2007, **316**, 102–105.
2 S. Ju, K. Lee and D. B. Janes, *Nano Lett.*, 2005, **5**, 2281–2286.
3 M. Law, D. J. Sirbuly, J. C. Johnson, J. Goldberger, R. J. Saykally and P. Yang, *Science*, 2004, **305**, 1269–1273.
4 M. H. Huang, S. Mao, H. Feick, H. Yan, Y. Wu, H. Kind, E. Weber, R. Russo and P. Yang, *Science*, 2001, **292**, 1897–1899.
5 F. Favier, E. C. Walter, M. P. Zach, T. Benter and R. M. Penner, *Science*, 2001, **293**, 2227–2231.
6 A. J. Yin, J. Li, W. Jian, A. J. Bennett and J. M. Xu, *Appl. Phys. Lett.*, 2001, **79**, 1039–1041.
7 K. Nielsch, R. B. Wehrspohn, J. Barthel, J. Kirschner, U. Gösele, S. F. Fischer and H. Kronmüller, *Appl. Phys. Lett.*, 2001, **79**, 1360–1362.
8 G. Sauer, G. Brehm, S. Schneider, K. Nielsch, R. B. Wehrspohn, J. Choi, H. Hofmeister and U. Gösele, *J. Appl. Phys.*, 2002, **91**, 3243–3247.
9 D. J. Sellmyer, M. Zheng and R. Skomski, *J. Phys.: Condens. Matter*, 2001, **13**, R433–R460.
10 H. Pan, H. Sun, C. Poh, Y. Feng and J. Lin, *Nanotechnology*, 2005, **16**, 1559–1564.
11 D. Xu, X. Shi, G. Guo, L. Gui and Y. Tang, *J. Phys. Chem. B*, 2000, **104**, 5061–5063.
12 A. L. Prieto, M. S. Sander, M. S. Martín-González, R. Gronsky, T. Sands and A. M. Stacy, *J. Am. Chem. Soc.*, 2001, **123**, 7160–7161.
13 D. Xu, Y. Xu, D. Chen, G. Guo, L. Gui and Y. Tang, *Chem. Phys. Lett.*, 2000, **325**, 340–344.
14 L. Li, Y. Yang, X. Huang, G. Li and L. Zhang, *Nanotechnology*, 2006, **17**, 1706–1712.
15 S. Phok, S. Rajaputra and V. P. Singh, *Nanotechnology*, 2007, **18**, 475601.
16 P. Zhou, D. Xue, H. Luo and X. Luo, *Nano Lett.*, 2002, **2**, 845–847.
17 L. Trahey, C. R. Becker and A. M. Stacy, *Nano Lett.*, 2007, **7**, 2535–2539.
18 R. Inguanta, S. Piazza and C. Sunseri, *Electrochim. Acta*, 2008, **53**, 5766–5773.
19 B. Sun, X. Jiang, S. Dai and Z. Du, *Mater. Lett.*, 2009, **63**, 2570–2573.
20 I. U. Schuchert, M. E. Toimil-Molares, D. Dobrev, J. Vetter, R. Neumann and M. Martin, *J. Electrochem. Soc.*, 2003, **150**, C189–C194.
21 X. Dou, G. Li, H. Lei, X. Huang, L. Li and I. W. Boyd, *J. Electrochem. Soc.*, 2009, **156**, K149–K154.
22 A. Ghahremaninezhad and A. Dolati, *J. Alloys Compd.*, 2009, **480**, 275–278.
23 Y. Konishi, M. Motoyama, H. Matsushima, Y. Fukunaka, R. Ishii and Y. Ito, *J. Electroanal. Chem.*, 2003, **559**, 149–153.
24 H. Nakao, H. Yamada, M. Satoh, H. Asoh, M. Nakao and T. Tamamura, *Appl. Phys. Lett.*, 1997, **71**, 2770–2772.
25 S. H. Xu, G. T. Fei, X. G. Zhu, B. Wang, B. Wu and L. D. Zhang, *Nanotechnology*, 2011, **22**, 265602.
26 A. Ailsa and A. Michael, Bravais rule, *A Dictionary of Earth Sciences*, 1999Encyclopedia.com.

